Numerical Heat Transfer, Part A: Applications: An International Journal of Computation and Methodology
Publication details, including instructions for authors and subscription information:
http://www.tandfonline.com/loi/unht20

Numerical Simulation for Variations of Airflow Induced by an Object Getting In and Out of a Workbench

Wu-Shung Fu, Suh-Jenq Yang
Published online: 29 Oct 2010.

To cite this article: Wu-Shung Fu, Suh-Jenq Yang (2001) Numerical Simulation for Variations of Airflow Induced by an Object Getting In and Out of a Workbench, Numerical Heat Transfer, Part A: Applications: An International Journal of Computation and Methodology, 39:6, 593-609, DOI: 10.1080/10407780117056

To link to this article: http://dx.doi.org/10.1080/10407780117056

Numerical Heat Transfer, Part A, 39:593–609, 2001

1040-7782/01 $12.00 + .00

NUMERICAL SIMULATION FOR VARIATIONS OF AIRFLOW INDUCED BY AN OBJECT GETTING IN AND OUT OF A WORKBENCH

Wu-Shung Fu
Department of Mechanical Engineering, National Chiao Tung University, Hsinchu, 30056, Taiwan, Republic of China

Suh-Jenq Yang
Department of Industrial Engineering and Management, Nan Kai Institute if Technology, Nantou, 542, Taiwan, Republic of China

The variations of airflow patterns induced by an object getting in and out of a workbench in a vertical laminar flow cleanroom are studied numerically. This subject is an important issue of microcontamination control for fabrication of precision devices. The characteristic of the variations of the airflow is dynamic and is a type of moving boundary problem. An arbitrary Lagrangian–Eulerian (ALE) kinematic description method is employed to describe the flow field, and a penalty finite element formulation with moving meshes is adopted to solve this problem. Three different moving speeds of the moving object with Reynolds number* Re *=500 are considered. The results show that the formation of recirculation zones, which inhibit removing contaminants, is remarkably dependent upon the moving speed of the object getting in and out of the workbench.

INTRODUCTION

Because of the demand of miniaturization of MEMS, biological sensors, semiconductor devices, and so on, a high-level cleanroom becomes an indispensable environment. To maintain the cleanliness of the cleanroom, the external air entering the cleanroom must be filtered by HEPA or ULPA filter banks. Thus, operators and equipment become major contaminative sources in the cleanroom. Most contaminants are continuously swept away by the airflow from the ceiling of the cleanroom. However, some residual particles, which may circulate within recirculation zones or deposit on the products and equipment, are extremely difficult to remove by the airflow. How to simulate the motion of the airflow and remove residual particles effectively is critical.

Received 29 February 2000; accepted 27 November 2000.
The support of this work by the National Science Council of Taiwan, Republic of China, under contract NSC89-2212-E-009-01 9 is gratefully acknowledged.
Address correspondence to Wu-Shung Fu, Department of Mechanical Engineering, National Chiao Tung University, 1001 Ta Hsuch Road, Hsinchu, Taiwan 30056, Republic of China. E-mail: wsfu@cc.nctu.edu.tw

NOMENCLATURE

h	dimensional height of the cleanroom [m]	v_1	dimensional airflow inlet velocity at section $\overline{AB}$ [m · s^{-1}]
H	dimensionless height of the cleanroom	V_1	dimensionless airflow inlet velocity at section $\overline{AB}$
h_0	dimensional height of the stationary object [m]	w	dimensional width of the cleanroom [m]
H_0	dimensionless height of the stationary object	W	dimensionless width of the cleanroom
h_1	dimensional distance from the outlet of the cleanroom to the stationary object [m]	w_0	dimensional width of the stationary object [m]
H_1	dimensionless distance from the outlet of the cleanroom to the stationary object	W_0	dimensionless width of the stationary object
h_2	dimensional distance from the workbench to the moveable part [m]	w_1	dimensional width of the airflow inlet at section $\overline{AB}$ [m]
H_2	dimensionless distance from the workbench to the moveable part	W_1	dimensionless width of the airflow inlet at section $\overline{AB}$
h_3	dimensional height of the moveable part [m]	w_2	dimensional width of the airflow inlet at section $\overline{CD}$ [m]
H_3	dimensionless height of the moveable part	W_2	dimensionless width of the airflow inlet at section $\overline{CD}$
h_4	dimensional height of the workbench [m]	w_3	dimensional width of the moveable part [m]
H_4	dimensionless height of the workbench	W_3	dimensionless width of the moveable part
n_e	number of elements	w_4	dimensional distance from the workbench to the stationary object [m]
p	dimensional pressure [N · m^{-2}]	W_4	dimensionless distance from the workbench to the stationary object
P	dimensionless pressure	x, y	dimensional Cartesian coordinates [m]
p_∞	reference pressure [N · m^{-2}]	X, Y	dimensionless Cartesian coordinates
Re	Reynolds number	ϕ	variables
t	dimensional time [s]	λ	penalty parameter
u, v	dimensional velocities of airflow in x- and y-directions [m · s^{-1}]	ν	kinematic viscosity [m · s^{-1}]
U, V	dimensionless velocities of airflow in X- and Y-directions	ρ	density [kg · m^{-3}]
u_b	dimensional moving velocity of the moveable part [m · s^{-1}]	τ	dimensionless time
U_b	dimensionless moving velocity of the moveable part	$\Delta\tau$	time step
$\hat{u}$	dimensional mesh velocity in x-direction [m · s^{-1}]	$[\ ]$	matrix
$\hat{U}$	dimensionless mesh velocity in X-direction	$\{\ \}$	column vector
v_0	dimensional airflow inlet velocity at section [m · s^{-1}]	$\langle\ \rangle$	row vector
V_0	dimensionless airflow inlet velocity at section $\overline{CD}$	$\lvert\ \rvert$	absolute value

Superscripts

(e)	element
m	iteration number
T	transpose matrix

Many studies have been performed on the motion of the airflow and particles. Ermak and Buckholz [1] adopted a Monte Carlo method to simulate the effects of the airflow on the particles, and the results showed that the characteristics of the particle transport were dominated by the airflow. Liu and Anh [2] used the analogy between the mass and heat transfers to determine the particle deposition rates by diffusion. Yamamoto [3] utilized a numerical method to study the interaction of the airflow within the cleanroom and the particle deposition mechanism in the work area. The results showed that a workbench obstructs the airflow, and recirculation zones were observed near the workbench. In addition, Lemaire and Luscuere [4] adopted a computer model to investigate the airflow and contaminant transports in the cleanroom. Marvell [5] summarized the factors of effects on the airflow and contaminant transports in a minienvironment system. Tannous [6] employed the computational fluid dynamics method to investigate the flow fields of a minienvironment system in the cleanroom.

However, for facilitating the analysis, most studies mentioned above regarded a moving operator or robot as a stationary object in the cleanroom, which resulted in the phenomena of the airflow being rather different from what actually occurs. Fu and colleagues [7] and Fu and Yang [8] adopted an ALE kinematic description method with finite element formulation to simulate the effect of a moving operator on the variations of the airflow and particles in the cleanroom. The results showed that large new recirculation zones were formed around the operator and work area because of the movement of the operator, and these phenomena were quite different from those that regarded the moving operator as stationary in the cleanroom.

In addition to the cleanroom, a workbench is indispensable for fabricating highly reliable quality precision products for the industires mentioned above. Therefore, the variations of the flow field in the workbench were investigated by many researchers [9–11]. A moveable part of an operator or robot, such as an arm, always gets in and out of the workbench while it performs its tasks, which affects the variations of flow field in the workbench remarkably. But this subject has been investigated minimally, and little literature is available.

Consequently, the purpose of this study is to numerically simulate the variations of the airflow induced by an object getting in and out of the workbench in the cleanroom. Because of the movement of the object, this subject is classified as a moving boundary problem, which is difficult to analyze solely using either the Lagrangian or Eulerian kinematic description method. An appropriate kinematic description of the ALE method is adopted to describe this problem. Details of the ALE method are given in Hirt et al. [12], Hughes et al. [13], and Ramaswamy [14]. A Galerkin finite element method with moving meshes and an implicit difference scheme, which deals with the time terms, is used to solve the governing equations. Three different moving speeds of the object are taken into consideration, and the results show that recirculation zones forming in the workbench are remarkably dependent on the moving speed of the object.

PHYSICAL MODEL

A two-dimensional vertical laminar flow cleanroom as sketched in Figure 1 is used. The width and height of the cleanroom are $w(= w_1 + w_2)$and h, respectively.

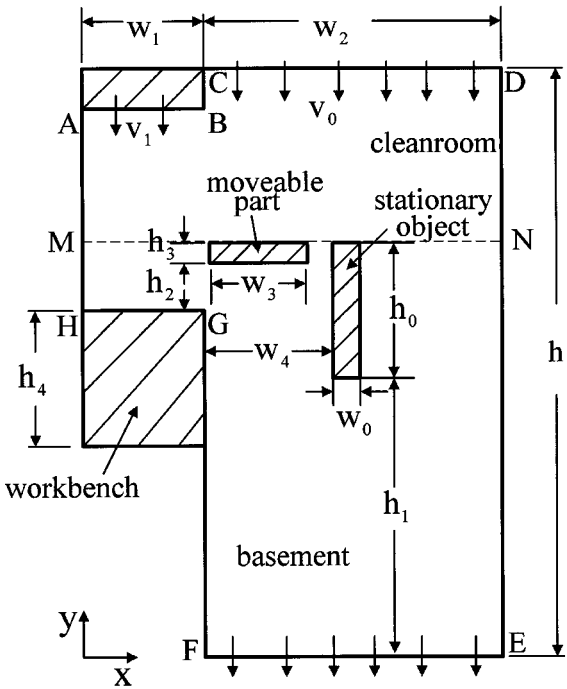

Figure 1. Physical model.

A stationary object, assumed to be an operator or a robot, and a moveable part, such as an arm of the operator or robot, are simulated by two rectangular blocks, respectively. The moveable part is conveniently named "arm" hereafter. Denote the height and width of the stationary object by h_0 and w_0, respectively, and the height and width of the arm by h_3 and w_3, respectively. A workbench with height h_4 and width w_1 is set on the left side of the cleanroom. The distance from the outlet of the cleanroom to the stationary object is h_1, and the distance from the workbench to the arm is h_2. Two different inlet velocities v_1 and v_0 of the airflow, where $v_1 > v_0$, flow through the inlet sections $\overline{AB}$ and $\overline{CD}$, respectively. Initially ($t = 0$), the objects stay beside the workbench and the airflow flows steadily. As time $t > 0$, the arm gets in the workbench with a constant velocity u_b and stays inside the workbench to perform tasks. Finally, the arm gets out of the workbench with a constant velocity u_b and goes back to its original place. The interaction between the airflow and arm affects the behavior of the airflow in the cleanroom. This subject is a type of moving boundary problem and becomes a time-dependent problem. Thus, it is best to use the ALE method to analyze this problem.

For facilitating the analysis, the following assumptions are made.

(1) The flow field is two-dimensional, incompressible, and laminar.
(2) The properties of the airflow are constant and the effect of gravity is ignored.

(3) The no-slip condition is held on the interfaces between the airflow and objects.

Based upon the characteristic scales of w_0, v_0, and ρv_0^2, the dimensionless variables are defined as follows:

$$\begin{aligned} X &= \frac{x}{w_0} \qquad Y = \frac{y}{w_0} \quad U = \frac{u}{v_0} \\ V &= \frac{v}{v_0} \qquad \hat{U} = \frac{\hat{u}}{v_0} \quad U_b = \frac{u_b}{v_0} \\ P &= \frac{p - p_\infty}{\rho v_0^2} \quad \tau = \frac{t v_0}{w_0} \quad \mathrm{Re} = \frac{v_0 w_0}{\nu} \end{aligned} \tag{1}$$

where $\hat{u}$ is the mesh velocity in the x-direction.

According to the above assumptions and dimensionless variables, the dimensionless ALE governing equations are expressed as following equations.

Continuity equation

$$\frac{\partial U}{\partial X} + \frac{\partial V}{\partial Y} = 0 \tag{2}$$

Momentum equations

$$\frac{\partial U}{\partial \tau} + (U - \hat{U})\frac{\partial U}{\partial X} + V\frac{\partial U}{\partial Y} = -\frac{\partial P}{\partial X} + \frac{1}{\mathrm{Re}}\left(\frac{\partial^2 U}{\partial X^2} + \frac{\partial^2 U}{\partial Y^2}\right) \tag{3}$$

$$\frac{\partial V}{\partial \tau} + (U - \hat{U})\frac{\partial V}{\partial X} + V\frac{\partial V}{\partial Y} = -\frac{\partial P}{\partial Y} + \frac{1}{\mathrm{Re}}\left(\frac{\partial^2 V}{\partial X^2} + \frac{\partial^2 V}{\partial Y^2}\right) \tag{4}$$

As the time $\tau > 0$, the boundary conditions are as follows.

On the wall surfaces $\overline{BC}$, $\overline{DE}$, $\overline{FG}$, $\overline{GH}$, and $\overline{AH}$,

$$U = V = 0 \tag{5}$$

On the inlet section $\overline{AB}$ (excluding point A),

$$U = 0 \qquad V = -1.25 \tag{6}$$

On the inlet section $\overline{CD}$ (excluding point D),

$$U = 0 \qquad V = -1.0 \tag{7}$$

On the outlet section $\overline{EF}$ (excluding the points E and F),

$$\partial U/\partial Y = \partial V/\partial Y = 0 \tag{8}$$

On the interfaces of the stationary object and the airflow,

$$U = V = 0$$

On the interfaces of the arm and the airflow,

$$U = U_b \qquad V = 0 \tag{10}$$

NUMERICAL METHOD

A Galerkin finite element formulation with moving meshes and an implicit scheme, dealing with the time terms, are adopted to solve the governing equations (2)–(4). The Newton–Raphson iteration algorithm and a penalty function model [15] are utilized to simplify the nonlinear and pressure terms in the momentum equations, respectively. The velocity terms are approximated by quadrilateral and nine-node quadratic isoparametric elements. The discretization processes of the governing equations are similar to the one used in Fu and colleagues [16]. Then the momentum equations (3)–(4) can be expressed as follows:

$$\sum_{1}^{n_e}([A]^{(e)} + [K]^{(e)} + \lambda[L]^{(e)})\{q\}^{(e)}_{\tau+\Delta\tau} = \sum_{1}^{n_e}\{f\}^{(e)} \tag{11}$$

where

$$(\{q\}^{(e)}_{\tau+\Delta\tau})^T = \langle U_1, U_2, \ldots, U_9, V_1, V_2, \ldots, V_9\rangle^{m+1}_{\tau+\Delta\tau} \tag{12}$$

$[A]^{(e)}$—mth iteration values of U and V at the time $\tau + \Delta\tau$,
$[K]^{(e)}$—shape function, $\hat{U}$, and time differential terms,
$[L]^{(e)}$—penalty function terms,
$\{f\}^{(e)}$—known values of U and V at the time and mth iteration values of U and V at the time $\tau + \Delta\tau$.

In Eq. (11), the terms with the penalty parameter λ are integrated by 2×2 Gaussian quadrature, and the other terms are integrated by 3×3 Gaussian quadrature. The value of the penalty parameter used in this study is 10^6, and the frontal method solver [17–19] is applied to solve Eq. (11).

The mesh velocity $\hat{U}$ is assumed to be linearly distributed and inversely proportional to the distance between the node and arm in this study. The mesh velocity near the arm is faster than that near the boundaries of the computational domain. In addition, the boundary layer thickness on the object surface is extremely thin and can be estimated approximately by $1/\sqrt{\mathrm{Re}}$ [20]. To prevent the computational nodes in the vicinity of the arm from slipping away from the boundary layer, the mesh velocities adjacent to the arm are expediently assigned to be equal to the velocity of the arm.

A brief outline of the solution procedure is described as follows:

(1) Determine the optimal mesh distribution and number of the elements and nodes.
(2) Solve the values of U and V steady state and regard them as the initial values.
(3) Determine the time increment and the mesh velocities $\hat{U}$ at every node.
(4) Update the coordinates of the nodes and examine the determinant of the Jacobian transformation matrix to ensure that the one-to-one mapping is satisfied during the Gaussian quadrature numerical integration; otherwise, execute the mesh reconstruction.

(5) Solve Eq. (11) until the following criteria for convergence are satisfied:

$$\left|\frac{\phi^{m+1}-\phi^{m}}{\phi^{m+1}}\right|_{\tau+\Delta\tau} < 10^{-3} \qquad \text{where } \phi = U, V \tag{13}$$

(6) Continue the next time step calculation until the assigned position of the arm is reached.

RESULTS AND DISCUSSION

The dimensionless geometric parameters in Table 1 are used in this study. Three different moving speeds 4.0, 2.0, and 0.5, which correspond to cases 1, 2 and 3, respectively, of the arm with Reynolds number $\mathrm{Re} = 500$, are considered in detail.

To obtain the optimal computational mesh, three different nonuniform distribution elements 3192, 3408, and 3876 (corresponding to 13111, 13979, and 15833 nodes, respectively) are used for the mesh tests at the steady state and $\mathrm{Re} = 500$ situations. The results of the velocities U and V distributions along the line $\overline{MN}$ as shown in Figure 1 are indicated in Fig 2. According to the results of the mesh tests, the computational mesh with 3876 elements is adopted. As for the selection of the time step $\Delta\tau$, three different time steps 0.05, 0.01, and 0.005 at $\mathrm{Re} = 500$ and the moving velocity of the arm $U_b = -2.0$ are executed. Similarly, the distributions of the velocities U and V along the line $\overline{MN}$ at time $\tau = 0.5$ are shown in Figure 3. The variations of the velocities U and V of the above different time steps are consistent, and the time step $\Delta\tau = 0.01$ is chosen.

To illustrate the variations of the airflow in more detail, we only present the velocity vectors around the workbench. Besides, the velocity vectors shown in the following figures are scaled relative to the maximum velocity in the flow field.

The transient developments of the velocity vectors for case 1are shown in Figure 4. In this case, the moving speed of the arm is 4.0. This speed is approximately equal to that of the arm of the robot moving to the workbench to pick up the products. At the time $\tau = 0.0$, as shown in Figure 4*a*, the arm is stationary and the airflow flows steadily. Recirculation zones, in which the particles are suspended and are difficult to remove, are observed apparently near the bottom surface of the arm and left corner of the top surface of the workbench. As the time $\tau > 0.0$, the arm gets in the workbench with a constant velocity $U_b = -4.0$. Thus, the variations of the flow field become transient. As shown in Figure 4*b*, the arm presses the airflow near the left side of the arm, and the flowing direction of the airflow is forced to change and turn to the bottom surface of the arm. As

Table 1. The dimensionless geometric lengths of the vertical laminar flow cleanroom

W_0	W_1	W_2	W_3	W_4	H	H_0	H_1	H_2	H_3	H_4
1.0	2.5	7.5	1.5	2.5	34.0	5.0	22.0	1.5	0.5	4.0

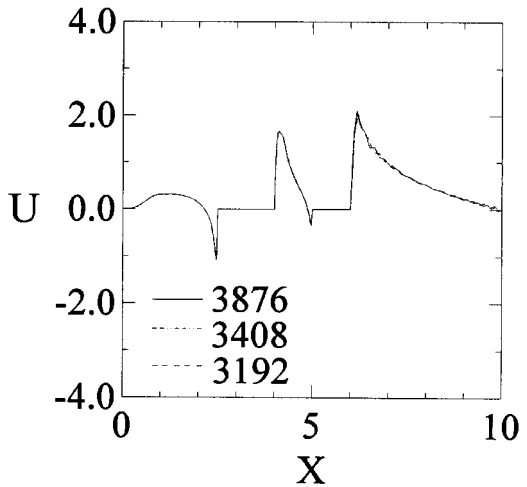

(a)

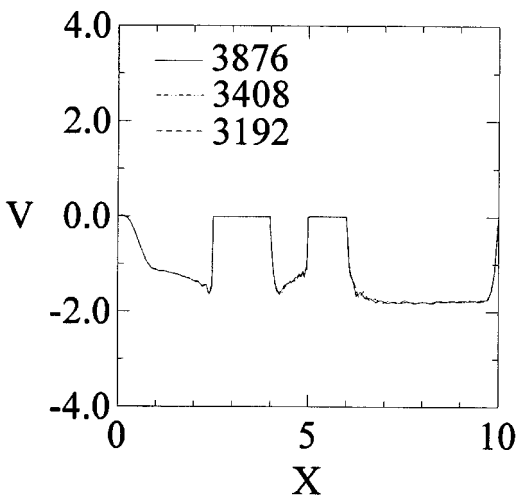

(b)

Figure 2. Comparison of the distribution of the velocities U and V along the line $\overline{MN}$ at the steady state and $\mathrm{Re} = 500$ for various meshes (*a*) $X - U$, (*b*) $X - V$.

a result, a new small recirculation zone is found around the left bottom corner of the arm. As for the airflow near the region of the right side of the arm, it simultaneously replenishes the vacant space induced by the movement of the arm. Consequently, recirculation zones are formed around this region. Besides, the recirculation zones around the bottom surface of the arm at the steady state are shrunk gradually because of the movement of the arm. As the time increases, as shown in

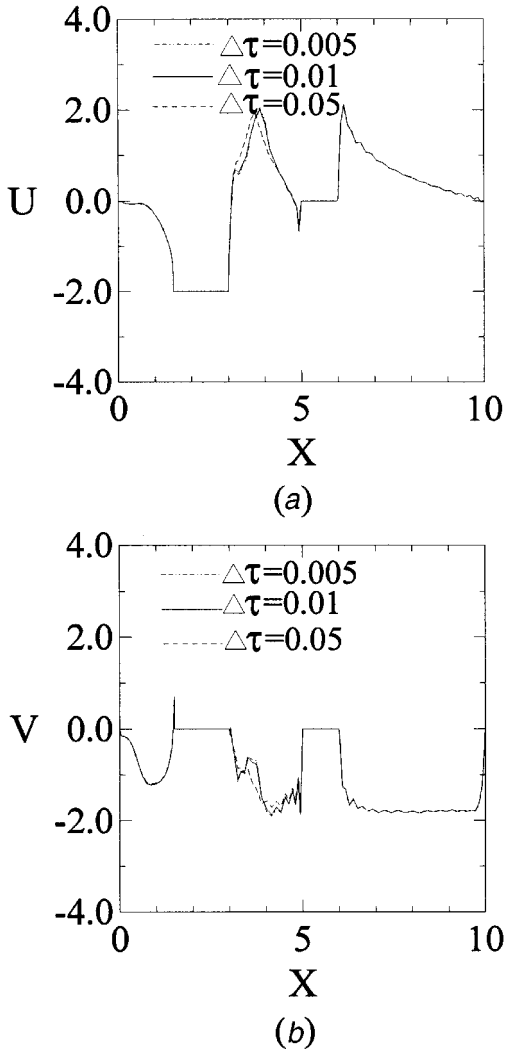

Figure 3. Comparison of the distribution of the velocities U and V along the line $\overline{MN}$ for various time steps under the moving velocity of the arm $U_b = -2.0$ and $\mathrm{Re} = 500$ at time $\tau = 0.5$. (*a*) $X - U$, (*b*) $X - V$.

Figures 4*c*–4, because the space between the arm and left wall of the workbench becomes narrower, the velocity of the airflow flowing through this space will increase. Thus, the airflow flowing through this space destroys the recirculation zone around the left corner of the top surface of the workbench. Conversely, the recirculation zone around the left bottom corner of the arm enlarges gradually and extends to the right of the bottom surface of the arm.

During the time τ from 0.5 to 1.5, as shown in Figures 4*e*–4*f*, we assume that the arm stays inside the workbench ($U_b = 0.0$). The recirculation zone near the

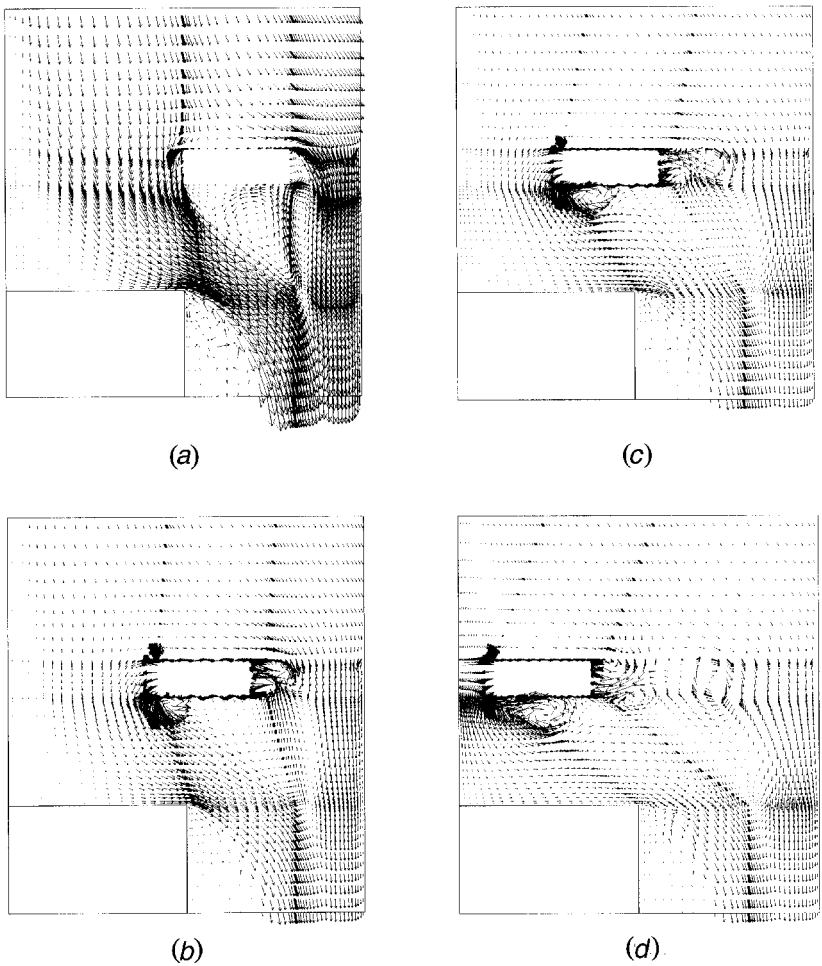

Figure 4. Transient developments of the velocity vectors around the workbench for case 1. (*a*) $\tau = 0.0$, $U_b = 0.0$; (*b*) $\tau = 0.1$, $U_b = -4.0$; (*c*) $\tau = 0.25$, $U_b = -4.0$; (*d*) $\tau = 0.5$, $U_b = -4.0$; (*e*) $\tau = 1.0$, $U_b = 0.0$; (*f*) $\tau = 1.5$, $U_b = 0.0$; (*g*) $\tau = 1.75$, $U_b = 4.0$; (*h*) $\tau = 2.0$, $U_b = 4.0$.

right side of the arm vanishes gradually, but the recirculation zones around the bottom surface of the arm still enlarge and extend to the top surface of the workbench, which is disadvantageous to the products on the workbench. In addition, because the airflow separately flows around the left and right sides of the arm, new recirculation zones are observed around the right corner of the workbench, as indicated in Figure 4*f*.

As the time $\tau > 1.5$, the arm gets out of the workbench with a constant velocity $U_b = 4.0$, as shown in Figures 4*g*–4h. Because the space between the arm and the left wall of the workbench gradually becomes broad, the inlet airflow can pass easily through this space. As a result, in Figure 4*h* the recirculation zones forming above the top surface of the workbench shrink gradually. As for the region near the left

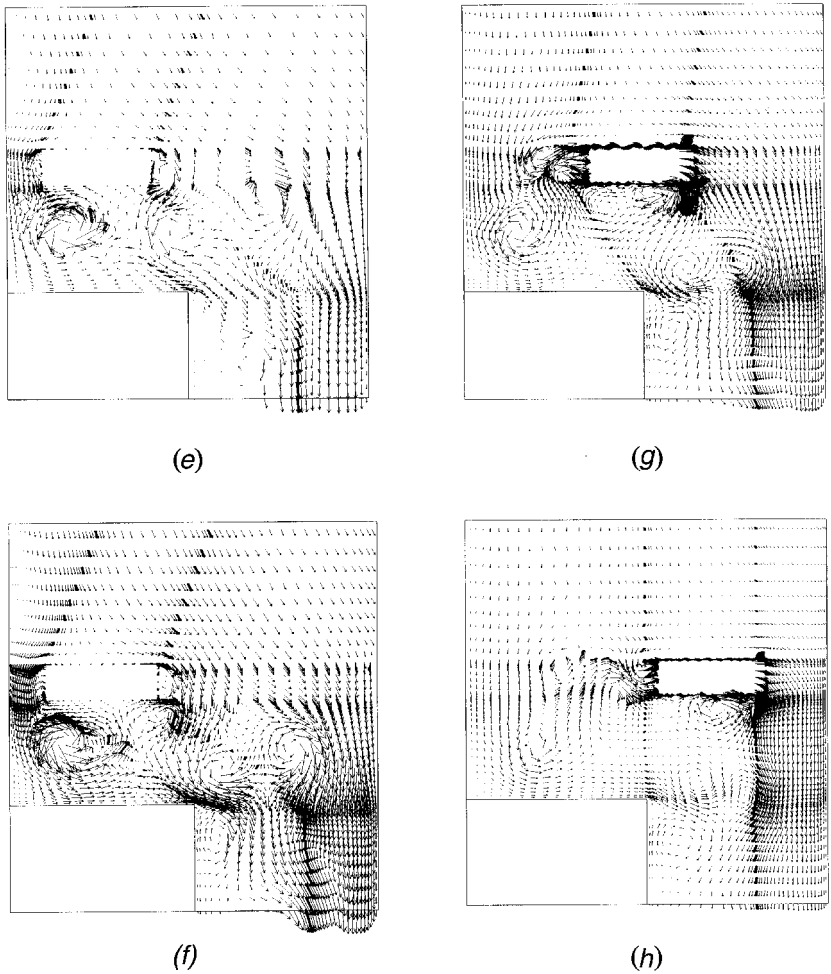

Figure 4. (*continued*).

side of the arm, the airflow, which combines with the inlet airflow and reverse airflow on the top surface of the workbench, replenishes the vacant space near the left side of the arm induced by the movement of the arm. On the other hand, because the moving velocity of the arm is fast, the airflow near the right side of the arm is pressed by the arm and turned to flow toward the bottom surface of the arm. Thus, a new recirculation zone forms around the right corner of the bottom surface of the arm.

Figure 5 shows the transient developments of the velocity vectors around the workbench for case 2. In this case, the moving speed of the moveable part is 2.0. In the first stage of the transient state, as shown in Figures 5*b*–5(*c*), the arm moves toward the workbench with a constant velocity $U_b = -2.0$, which is slower than that of the above case. As the arm moves toward the left, the recirculation zone around the bottom surface of the arm is larger and more apparent than that of

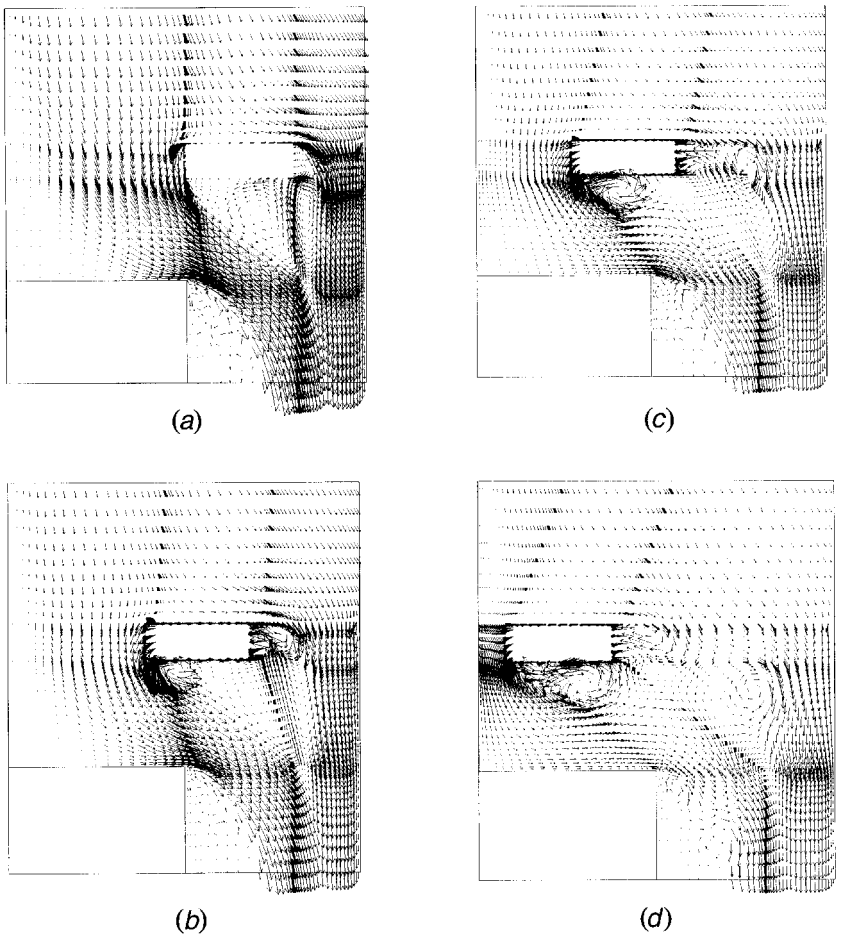

Figure 5. Transient developments of the velocity vectors around the workbench for case 2. (*a*) $\tau = 0.0$, $U_b = 0.0$; (*b*) $\tau = 0.2$, $U_b = -2.0$; (*c*) $\tau = 0.5$, $U_b = -2.0$; (*d*) $\tau = 1.0$, $U_b = -2.0$; (*e*) $\tau = 1.5$, $U_b = 0.0$; (*f*) $\tau = 2.0$, $U_b = 0.0$, (*g*) $\tau = 2.5$, $U_b = 2.0$; (*h*) $\tau = 3.0$, $U_b = 2.0$.

case 1. The results are remarkably different from the results of Fu and colleagues [7], which indicated that an operator with a slower moving speed might form small recirculation zones around the operator and workbench.

During the time τ from 1.0 to 2.0, as shown in Figures 5*e*–5*f*, the arm stays inside the workbench ($U_b = 0.0$). The recirculation zones around the top surface of the workbench enlarge gradually and extend to the top surface of the workbench closely, which are similar to the above case.

As the time $\tau > 2.0$, the arm leaves the workbench with a constant velocity $U_b = 2.0$, as shown in Figures 5*g*–5*h*. As the time increases, most of the airflow, which replenishes the vacant space induced by the movement of the arm, is not supplied directly from the inlet airflow, but from the airflow flowing over the top surface of the workbench. The variations of the flow field affected by the inlet airflow and

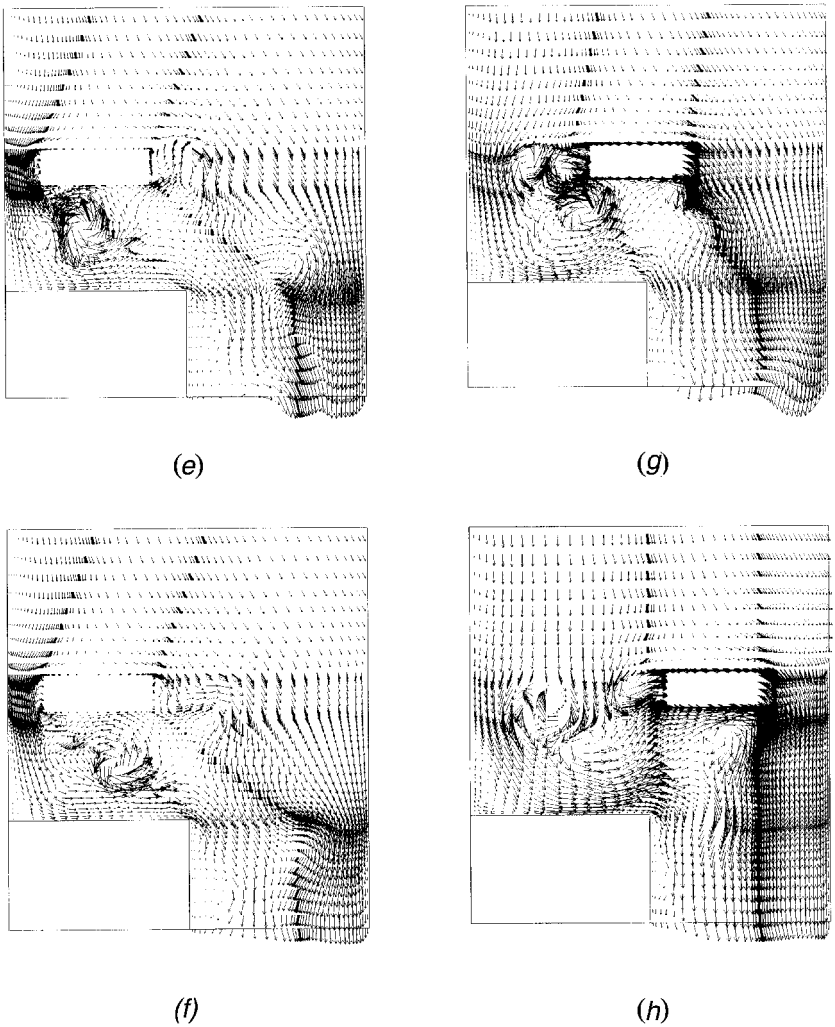

Figure 5. (*continued*)

recirculation zones mentioned above are more drastic than those of the above case. In Figure 5*h*, the recirculation zones near the right corner of the workbench and bottom surface of the arm are destroyed by the airflow flowing over the top surface of the workbench and vanish gradually. These phenomena are different from the above case.

The transient developments of the velocity vectors around the workbench for case 3, in which the moving speed of the arm is slower and equal to 0.5, are shown in Figure 6. Because the velocity of the inlet airflow is larger than the moving velocity of the arm, the arm seems to be an obstruction in the way of the airflow. The vacant space induced by the movement of the arm is replenished by the inlet airflow instantly. In the meantime, some of the inlet airflow circumvents the right side

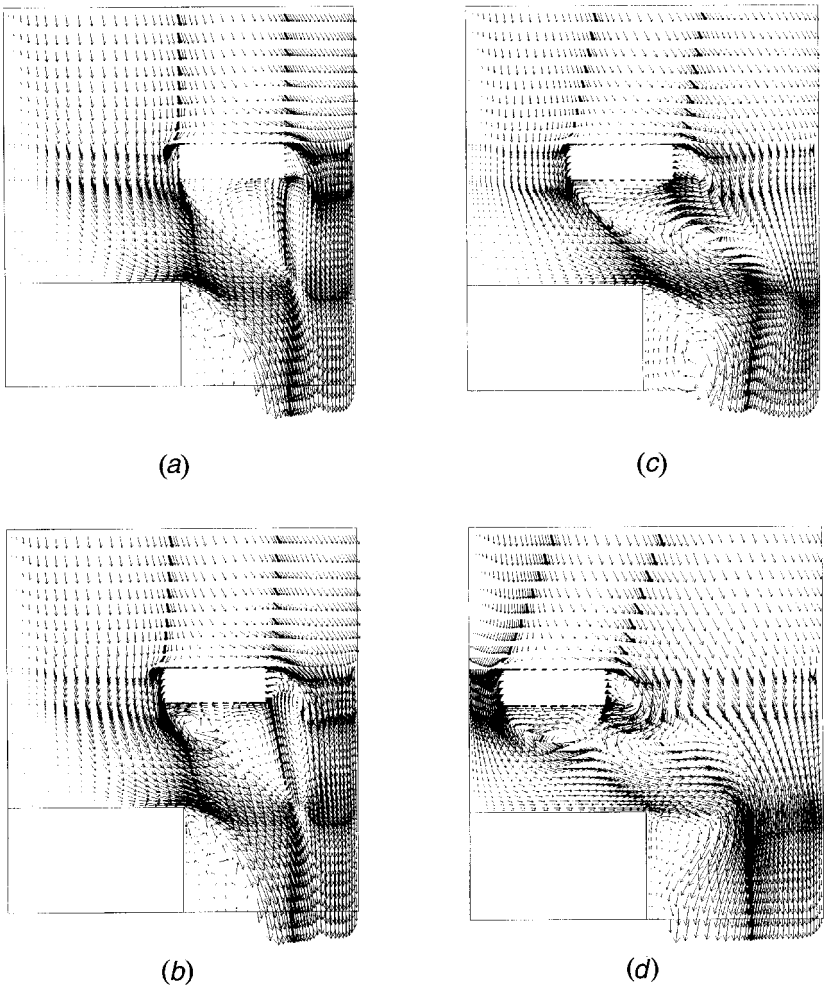

Figure 6. Transient developments of the velocity vectors around the workbench for case 3. (*a*) $\tau = 0.0$, $U_b = 0.0$; (*b*) $\tau = 0.5$, $U_b = -0.5$; (*c*) $\tau = 1.0$, $U_b = -0.5$; (*d*) $\tau = 2.0$, $U_b = -0.5$; (*e*) $\tau = 2.5$, $U_b = 0.0$; (*f*) $\tau = 3.0$, $U_b = 0.0$; (*g*) $\tau = 4.0$, $U_b = 0.5$; (*h*) $\tau = 5.0$, $U_b = 0.5$.

of the arm and interacts with the airflow flowing through the left side of the arm. As a result, recirculation zones are observed near the bottom surface of the arm and are indicated in Figure 6*c*–d. The variations of the flow field are different from the above cases.

During the time τ from 2.0 to 3.0, as shown in Figures 6*e*–6*f*, the arm stays inside the workbench ($U_b = 0.0$). The recirculation zones mentioned above enlarge gradually and extend to close the top surface of the workbench, which is similar to the above cases.

In Figures 6*g*–6*h*, the arm gets out of the workbench with a constant velocity $U_b = 0.5$. As the time increases, the space between the arm and left side of the work-

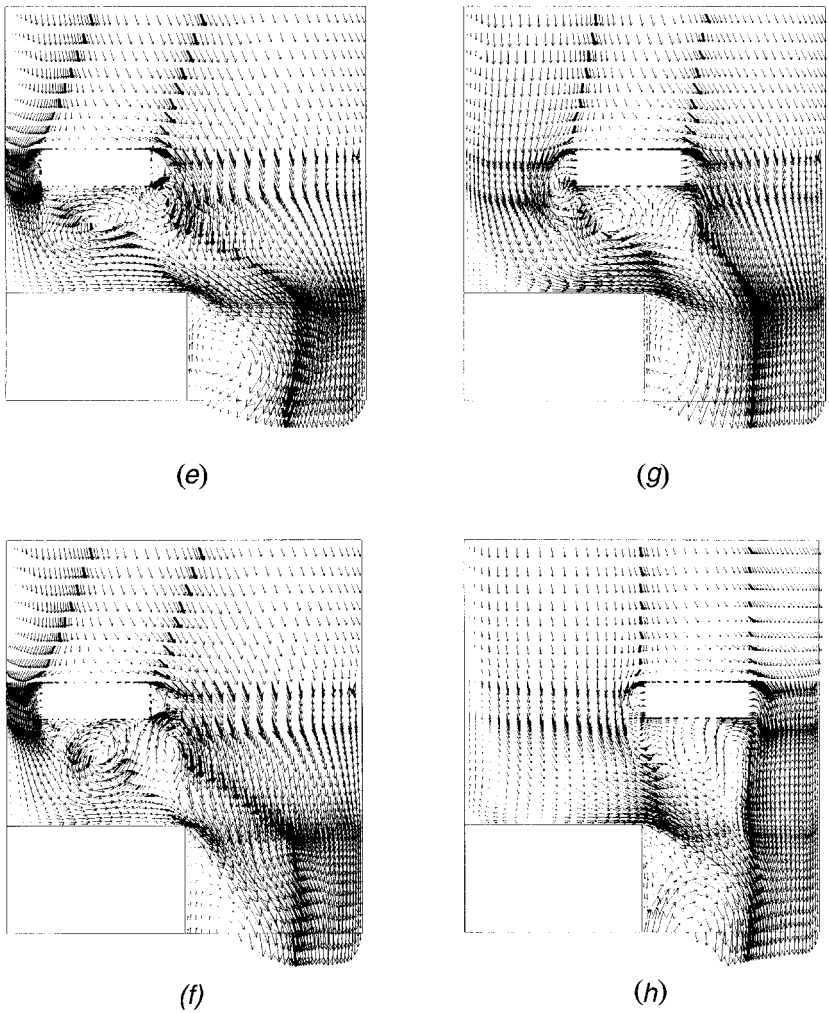

Figure 6. (*continued*).

bench becomes broad, and the inlet airflow easily passes through this space and replenishes the vacant space near the left side of the arm because of the movement of the arm. As shown in Figure 6*h*, the recirculation zones above the top surface of the workbench are almost destroyed by the inlet airflow, which is beneficial to the process.

CONCLUSIONS

A numerical investigation of the variation of the airflow patterns induced by an arm getting in and out of a workbench in a cleanroom is performed. The main conclusions can be summarized as follows:

(1) Several recirculation zones are observed around the arm as the arm gets in the workbench. More specifically, one of these zones near the bottom surface of the arm enlarges and extends gradually to cover the top surface of the workbench. These recirculation zones may entrain and trap the particles, which are disadvantageous to the products.
(2) As the arm gets in the workbench with faster, the smaller recirculation zone is formed around the workbench. Conversely, the arm getting out of the workbench more slowly can destroy the recirculation zones around the workbench.

REFERENCES

1. D. L. Ermak and H. Buckholz, Numerical Integration of the Langerin Equation: Monte Carlo Simulation, *J. Comput. Phys.*, vol. 35, pp. 169–182, 1980.
2. B. Y. H. Liu and K. Anh, Particle Deposition on Semiconductor Wafers, *Aerosol Science and Technology*, vol. 6, pp. 215–224, 1987.
3. T. Yamamoto, Airflow Modeling and Particle Control by Vertical Laminar Flow, in R. P. Donovan (ed.), *Particle Control for Semiconductor Manufacturing*, pp. 301–323, Marcel Dekker, New York, 1990.
4. T. Lemaire and P. Luscuere, Investigating Computer Modeling of Cleanroom Airflow Patterns, *Microcontamination*, vol. 9, pp. 19–26, 1991.
5. G. Marvell, Minienvironment Air Flow Dynamics, *Solid State Technology*, vol. 36, pp. 47–48, 1993.
6. A. G. Tannous, Air Flow Simulation in a Minienvironment, *Solid State Technology*, vol. 39, pp. 201–209, 1996.
7. W. S. Fu, S. F. Chen, and S. J. Yang, Numerical Simulation of Effects of Moving Operator on Removing of Particles in Cleanroom, to appear in *Aerosol and Air Quality Research*.
8. W. S. Fu and S. J. Yang, Numerical Study of Effects of Moving Operator and Curtain on Airflow Patterns in Cleanroom, submitted for publication.
9. J. Koenigsberg and E. W. Seipp, Laboratory Fume Hood, *ASHREA Journal*, vol. 30, pp. 43–46, 1988.
10. G. T. Saunder, Fume Hood Testing and Evaluation, *Journal of Chemical Education*, vol. 67, pp. 226–230, 1990.
11. F. Durstand and J. C. F. Pereira, Experimental and Numerical Investigations of the Performance of Fume Cupboards, *Building and Environment*, vol. 26, pp. 153–164, 1991.
12. C. W. Hirt, A. A. Amsden, and H. K. Cooks, An Arbitrary Lagrangian-Eulerian Computing Method for All Flow Speeds, *J. Comput. Phys.*, vol. 14, pp. 227–253, 1974.
13. T. J. R. Hughes, W. K. Liu, and, T. K. Zimmermann, Lagrangian-Eulerian Finite Element Formulation for Incompressible Viscous Flows, *Comput. Meth Appl. Mech. Eng.*, vol. 29, pp. 329–349, 1981.
14. B. Ramaswamy, Numerical Simulation of Unsteady Viscous Free Surface Flow, *J. Comput. Phys.*, vol. 90, pp. 396–343, 1990.
15. J. N. Reddy and D. K. Gartling, *The Finite Element Method in Heat Transfer and Fluid Dynamics*, pp. 145–151, CRC Press, Ann Arbor, MI, 1994.
16. W. S. Fu, T. M. Kau, and W. J. Shieh, Transient Laminar Natural Convection in an Enclosure from Steady Flow State to Stationary State, *Numerical Heat Transfer, Part A*, vol. 18, pp. 189–211, 1990.
17. B. M. Irons, A Frontal Solution Program for Finite Element Analysis, *Int. J. Num. Meth. Eng.*, vol. 2, pp. 5–32, 1970.

18. P. Hood, Frontal Solution Program for Unsymmetric Matrices, *Int. J. Num. Meth. Eng.*, vol. 10, pp. 379–399, 1976.
19. C. Taylor and T. G. Hughes, *Finite Element Programming of the Navier-Stokes Equations*, Chap. 6, Pineridge Press Ltd., U.K., 1981.
20. H. Schlichting, *Boundary Layer Theory*, 7th ed., Chap. 5, McGraw-Hill, New York, 1979.